

MICROSTRUCTURE OF AS-CAST HIGH-SILICON DUCTILE IRON PRODUCED VIA PERMANENT MOLD CASTING

Moritz Riebisch , Christoph Seiler, Björn Pustal, and Andreas Bührig-Polaczek
Foundry Institute, Rheinisch-Westfälische Technische Hochschule Aachen, Aachen, Germany

Copyright © 2018 American Foundry Society
<https://doi.org/10.1007/s40962-018-0232-5>

Abstract

Permanent mold casting of ductile iron is an environmentally friendly alternative to sand mold casting. The high cooling rate leads to a homogeneous microstructure with low grain size, but can also lead to cementite formation. In the work presented, the as-cast microstructure of solid solution-strengthened ductile iron (SSDI) cast in permanent mold made of gray iron is analyzed. The high silicon content in SSDI decreases chilling tendency and promotes the formation of ferrite. Silicon contents in the range 3.2–4.3 wt% and mold preheating temperatures in the range 300–450 °C were analyzed for section thicknesses of 10, 20 and 30 mm. Solidification time and cooling rate at the casting sections analyzed were measured. The results show that an as-cast microstructure free from carbides is achieved in sections of 20 and 30 mm for all

castings analyzed, whereas for 10 mm a partial chilled microstructure is produced. As expected, the pearlite content decreases with increasing silicon content and increasing preheating temperature. A higher cooling rate increases eutectoid undercooling and thus promotes pearlite formation. From the experiments carried out, a quantitative correlation is deduced for the pearlite content as a function of eutectoid undercooling and Si content. The nodule count is approximated as a linear dependency on solidification time.

Keywords: solid solution-strengthened ductile iron, permanent mold, silicon content, preheating temperature, microstructure, pearlite

Introduction

Ductile iron (DI) is a widely applied casting material with multiple benefits such as excellent castability, ductility and an ideal cost–performance ratio. It is an essential engineering material for automotive, machine building and wind power industry. Most ductile iron castings are produced in sand molds, whereas permanent mold casting of DI is only used for special applications of castings with rather simple geometry. The advantages of permanent mold casting are dimensional stability, superior surface finish, lower machining cost, finer grain size and the reduction in sand wastage.¹ On the contrary, the process is limited in terms of size, shape and section thickness of the casting and is only profitable for large batch sizes. The cooling rate in the permanent mold must be controlled to prevent the formation of cementite in DI. Cooling rate depends on section thickness, pouring temperature and preheating temperature of the mold. An increase in the silicon content reduces the

formation of carbides due to the higher graphitization potential.

The essential features of the solid solution-strengthened ductile iron grades (SSDI) with a silicon content between 3.2 and 4.3 wt% are the ferritic matrix and the unique combination of strength and ductility.² Above 4.3 wt% Si, the material becomes brittle due to silicon long-range ordering, which leads to the formation of DO₃-ordered phases.³ The impact of various alloying elements on microstructure and mechanical properties of SSDI has been reported in the recent past.^{4–6} The high Si content increases the tolerance against carbide-promoting elements and reduces the chilling tendency of the material which makes these grades convenient for permanent mold casting. Furthermore, the thermal conductivity of ferrite decreases with increasing Si content.⁷ However, critical conditions required to produce a fully ferritic matrix (< 5% pearlite) in the as-cast state have not yet been determined for SSDI

in permanent mold casting. In order to determine these conditions, the SSDI grades GJS-450-18, GJS-500-14 and GJS-600-10 with a respective silicon content of 3.2, 3.8 and 4.3 wt% are cast in a gray iron permanent mold with different section thicknesses varying the preheating temperature between 300 and 450 °C (572 and 842 °F). Cooling curves are recorded using thermocouples type K inside the mold to relate the microstructure to the cooling rate.

State of the Art

Permanent mold casting of DI has been investigated for several decades. Kitsudo et al.⁸ observed the microstructure of DI with Si concentrations in the range 2.5–4.7 wt% in a metal mold with 30 mm diameter. They obtained a complete ferritic matrix for 4.7% Si and elongation values up to 20% and concluded that it is possible to produce as-cast ferritic DI by permanent mold casting if a hyper-eutectic melt along with a high Si content is used. Later Kitsudo et al. described the impact of the carbon equivalent (CE) on the shrinkage cavity formation of hyper-eutectic DI cast in metal molds. According to their results, shrinkage cavities occur when the CE exceeds a critical value. The lowest CE where shrinkage cavities occur decreases when the carbon content is lowered and Si is increased. For 3.1 wt% C, no sound castings are produced regardless of the carbon equivalent. Khalil-Allafi and Amin-Ahmadi⁹ investigated the impact of Si contents between 2.1 and 3.3 wt% and preheating temperatures between 200 and 450 °C (392 and 842 °F) on the microstructure of DI in a gray iron mold with a section thickness of 20 mm. They showed that different combinations of both parameters are suitable to produce DI with neither carbides nor porosity. A high graphite nodule count is important to prevent the formation of chill according to Pengju et al.¹⁰ According to their study, a pre-treatment with Al and graphite and an inoculation with a Bi-containing inoculant lead to a significant increase in nodule count which again leads to a fully ferritic microstructure and good mechanical properties. The solidification time of DI in a permanent mold is studied by Narendranath and Srinivasan¹¹ and depends on graphite morphology and cooling rate. Variations of cooling rate can be achieved by changes in casting size, mold wall thickness or mold preheating temperature. Current examples for the application of ductile iron permanent mold castings are front-wheel hubs for heavy-load trucks as indicated by Zhuyao and Sizeng¹² and hydraulic manifolds, where solid solution-strengthened DI is used according to Herfurth et al.¹³ For the new SSDI grades, no experimental investigations have yet been reported where cooling conditions in permanent mold casting are linked to the microstructure. In the present study, the as-cast microstructure of SSDI in a permanent mold is analyzed for different cooling rates and Si contents to determine suitable conditions for a fully ferritic matrix in the as-cast

state and thus to promote the application of these DI grades in permanent mold casting.

Experimental Procedure

Design of Experiment

The gray iron permanent mold consists of two machined blocks with a vertical parting line. Figure 1 shows the cavity of the step-wedge die. The thickness of the steps is 10, 20 and 30 mm, respectively. The width and the height of each step are 100 and 60 mm, respectively. The step wedge is filled with melt from bottom to top. The mold is equipped with holes to place a thermocouple in each respective step to correlate the cooling behavior with the resulting microstructure. Mold filling simulations were performed prior to the production of the mold to ensure a laminar filling of the cavity.

The SSDI grades GJS-450-18 (3.2 wt% Si), GJS-500-14 (3.8 wt% Si) and GJS-600-10 (4.3 wt% Si) are cast with a carbon equivalent of approximately 4.50 and for mold preheating temperatures of 300, 350, 400 and 450 °C. This variation results in 12 experiments according to a factorial design of experiment. Table 1 shows the process data of all casting trials. The carbon content is determined via thermal analysis (TA) and the silicon content via optical emission spectrometry (OES). The concentration of other important elements in the melt is aimed at Mn = 0.17 wt%, Cr = 0.05 wt%, P = 0.02 wt% and Mg = 0.03 wt% for all casting trials.

Casting Procedure

The interior of the permanent mold is coated with a silica insulating mixture before every casting trial to ensure an easy ejection of the casting. The mold is heated with a gas burner before applying the coating with a brush. Three K type thermocouples were placed inside the mold before it is put into the furnace to reach the desired preheating temperature. Thermocouples with exposed measuring tips are used for a minimum response time. The thermocouples were always located in the center of each step.

For the production of the base melt recycled nodular iron feeders, EN-GJS-400-15 and high-purity iron 99.8% are melted with a medium-frequency induction furnace in a 50-kg graphite crucible. The silicon concentration is adjusted by alloying with ferrosilicon (75 wt% Si). The melt is superheated to 1520 °C (2768 °F), and then, slag is removed. The crucible is then lifted out of the furnace, and magnesium treatment is performed with a cerium-free FeSiMg master alloy in a plunger at a temperature of approximately 1500 °C (2732 °F). A second slag removal is performed after the magnesium treatment. Then, the melt

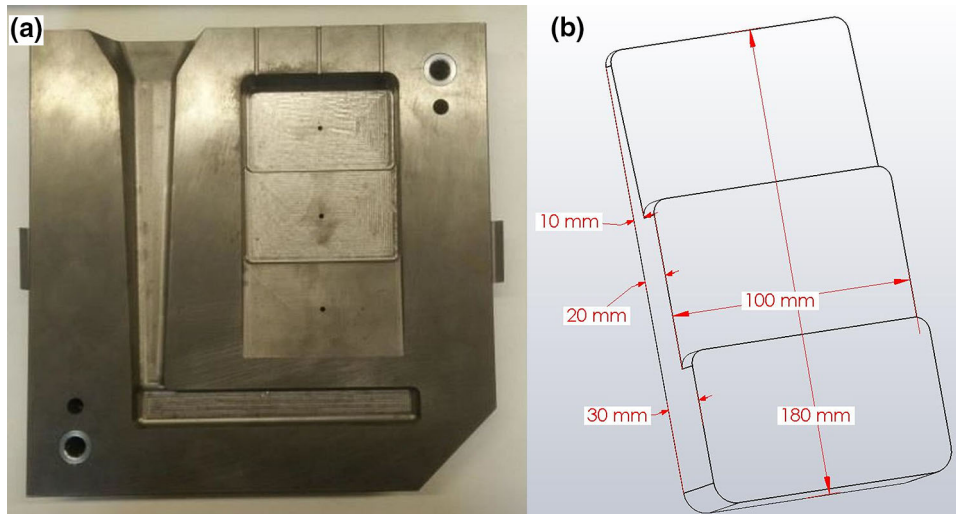


Figure 1. One part of the gray iron die showing the geometry of the step wedge, the downsprue and the runner (a) and dimensions of the cast part (b).

Table 1. Parameters Varied in the Factorial Design of Experiment for 12 Casting Trials

Cast no.	C (wt%)	Si (wt%)	CE	T preheat (°C)	T cast (°C)
1	3.30	3.15	4.35	297	1385
2	3.09	3.76	4.34	299	1380
3	2.84	4.36	4.29	298	1404
4	3.35	3.11	4.38	350	1390
5	3.10	3.96	4.42	344	1363
6	2.91	4.37	4.36	340	1368
7	3.30	3.20	4.37	392	1395
8	3.11	3.85	4.39	396	1410
9	3.00	4.43	4.48	394	1389
10	3.35	3.37	4.47	443	1374
11	3.17	3.96	4.49	438	1396
12	2.95	4.50	4.45	442	1374

is inoculated with 0.2 wt% of a ferrosilicon-based inoculant (approximately 65% Si, 2% Ca, 1% Bi and 1% RE) by stirring in the crucible. A chilled sample for chemical analysis is taken from the melt after inoculation. Furthermore, two thermal analysis cups are filled with the inoculated melt. Casting temperature is measured with a measuring rod before the melt is poured into the permanent mold. Additionally, a Y-shaped wedge with a wall thickness of 25 mm in a green sand mold is cast to control the mechanical properties of the material according to DIN EN 1563. Figure 2 shows the recorded cooling curves in the permanent mold for one of the casting trials. The Fe–Fe₃C eutectoid temperature determined via thermal analysis is marked with a horizontal broken line. From the cooling curves, it can already be concluded that primary cementite precipitated in the smallest step (10 mm wall thickness), whereas the other two curves indicate a stable graphite/

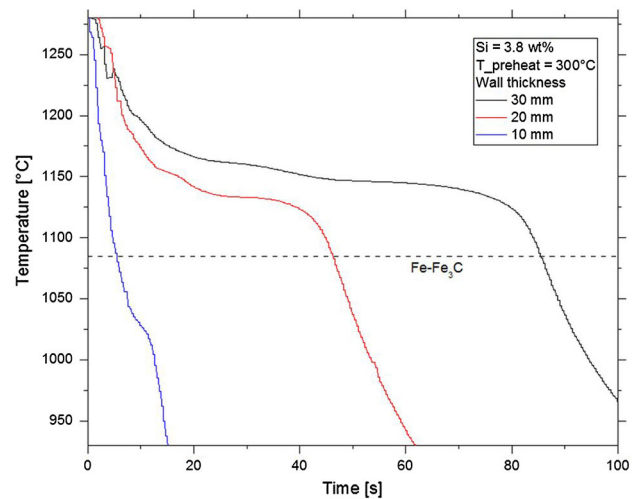


Figure 2. Representative cooling curves recorded in the center of each step (3.8 wt% Si, 300 °C preheating temperature).

austenite eutectic solidification. This is confirmed by metallographic analysis (see Figure 3). The casting is ejected from the permanent mold after the eutectoid transformation was finished in each part of the step wedge.

Specimen Analysis

The specimens for metallographic analysis are cut from the castings with a bow saw and a water-cooled disk cutter. The specimens are embedded in silicone molds (diameter 50 mm) with a cold-hardened potting compound. The embedded specimens are ground with SiC sandpaper with different grits (180, 320, 500 and 1000) and then polished with diamond polish (size 9, 3 and 0.25 μm). An automatic buffing machine is used for all grinding and polishing steps. The specimens are analyzed in the polished state for graphite analysis with a light optical microscope and later

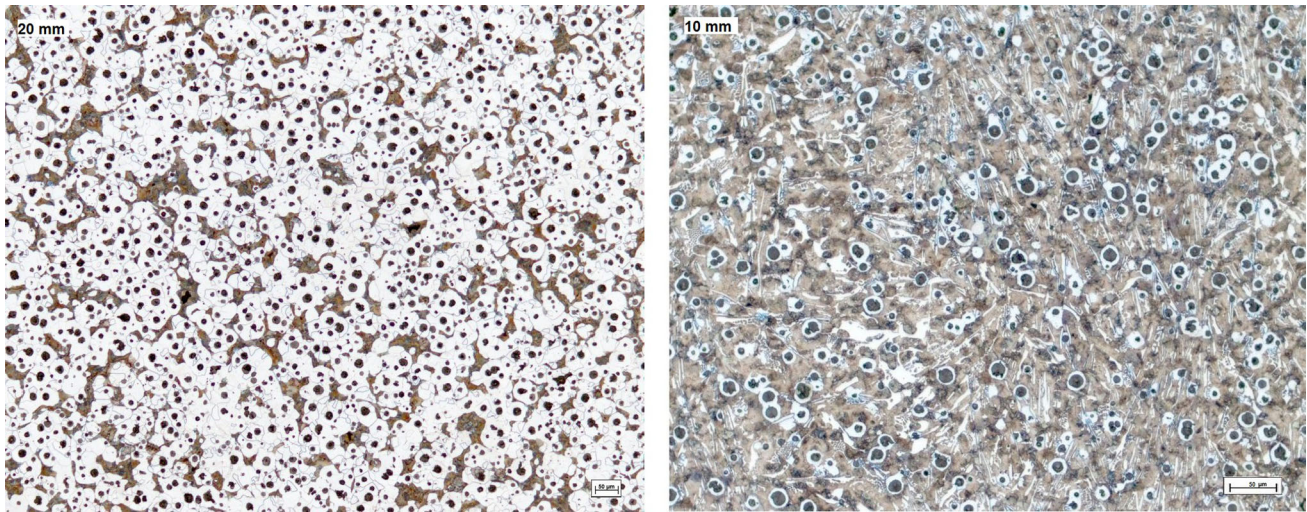


Figure 3. Microstructure in the 20- and 10-mm section for cast number 2. Carbides are present in the 10-mm-thick section, while the 20-mm section is free from carbides with a predominantly ferritic matrix.

after etching with alcoholic nitric acid to determine the pearlite content. Figure 3 shows exemplary pictures for etched samples from the 10- and 20-mm-thick section. Five pictures were taken for graphite and pearlite analysis with a magnification factor of 100 and a digital resolution of 2600×2060 pixels for specimens taken from the 30- and 20-mm-thick section. The image processing software Axiovision KS 400 is used for the quantitative evaluation of the pictures. Graphite shape and nodularity are determined according to the standard ASTM E2567-16a. Nodularity is calculated from the area A of graphite particles (class I–VI) according to

$$\text{Nodularity} = \frac{A_{VI} + 0.9 * A_V}{A_{I-VI}} \quad \text{Eqn. 1}$$

Only graphite particles with a minimum Ferret's diameter of $5 \mu\text{m}$ are considered for the evaluation of graphite nodule count and nodularity. This minimum nodule size is proposed by Ruxanda et al.¹⁴ for thin-wall ductile iron castings. To determine the area percentage of pearlite, the joint area percentage of graphite %G and pearlite %P is determined from the etched specimen. Then, the graphite area percentage evaluated from the polished samples is subtracted from it to determine the pearlite area percentage according to

$$\%P = (\%G + \%P)_{\text{etched}} - \%G_{\text{polished}} \quad \text{Eqn. 2}$$

The tensile properties are tested in the separately cast Y_{II} wedges by drilling out cores with a diameter of 15 and 120 mm length with a hollow drill. From the cores, the tensile test bars of shape type A with diameter 8 mm according to DIN EN 50125 are manufactured with a lathe.

Results and Discussion

The tensile test results indicate that the desired mechanical properties for SSDI according to DIN EN 1563 were achieved in all 12 casting trials. In Table 2, the averaged mechanical properties are listed.

The recorded cooling curves indicate that a chilled microstructure is always present in the 10-mm-thick section of the step wedge regardless of the Si content and the preheating temperature. Therefore, graphite morphology and pearlite fraction were only analyzed in the 20- and 30-mm-thick section. The results of microstructural analysis are listed in Table 3. The pearlite content refers to the area percentage of the metallic matrix. The nodule count ranges from approximately 500 to 750 nodules per mm^2 and is always higher in the 20-mm-thick than in the 30-mm section. Nodularity varies between 73 and 83% and is higher in the 30-mm section for most casting numbers.

Table 2. Averaged Mechanical Properties of SSDI Casted in Green Sand Molds

Cast no.	Tensile strength (MPa)	Yield strength (MPa)	Elongation (%)	Material
1, 4, 7, 10	501	357	22.2	EN-GJS-450-15
2, 5, 8, 11	545	416	19.5	EN-GJS-500-14
3, 6, 9, 12	603	481	15.8	EN-GJS-600-10

Table 3. Results of Microstructural Characterization

Cast no.	Wall thickness 20 mm			Wall thickness 30 mm		
	Nod. count (1/mm ²)	Nodularity (%)	Pearlite (%)	Nod. count (1/mm ²)	Nodularity (%)	Pearlite (%)
1	713	79.7	38.3	497	79.2	21.7
2	726	74.0	21.5	613	82.4	11.5
3	653	73.6	12.8	584	86.3	6.7
4	736	76.1	28.7	632	82.8	19.9
5	725	75.8	14.0	597	82.9	9.7
6	748	73.3	5.9	591	73.3	5.5
7	692	73.3	25.7	514	84.3	14.9
8	680	77.4	14.3	542	78.3	7.5
9	690	76.8	6.8	521	75.8	5.5
10	666	76.8	13.6	506	81.1	10.0
11	706	76.2	6.8	561	81.4	6.3
12	752	76.6	3.1	551	79.8	4.4

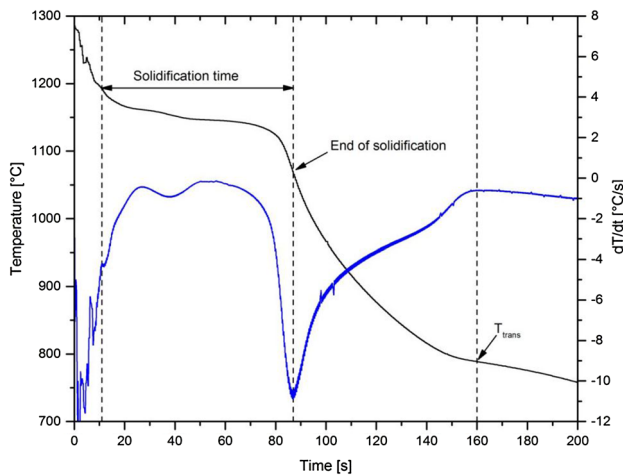


Figure 4. Cooling curve (black) and first derivative (blue) for cast number 2 in the 30-mm-thick section. Arrows indicate the solidification time, end of solidification and eutectoid transition temperature.

Figure 4 shows how solidification time and eutectoid transition temperature are determined by using first derivative cooling curve analysis. The solidification time is the interval between liquidus temperature and end of eutectic solidification. The transition temperature is determined at the maximum of the first derivative during eutectoid transformation. Cooling rate is determined between end of solidification and transition temperature. Table 4 shows the results of cooling curve analysis. Solidification time in the 20-mm-thick section ranges from 42 to 72 s and from 77 to 118 s in the 30-mm-thick section. A high solidification time is usually combined with a low cooling rate after solidification. Cooling rate varies between 2.2 and 4.4 °C/s in the 20-mm section and between 2.2 and 3.9 °C/s in the 30-mm section. The transition temperature, which indicates the beginning of the

solid-state transformation, is lower than the eutectoid equilibrium temperature because the presented high cooling rates cause a eutectoid undercooling. Transition temperature is always lower in the 20-mm section than in the 30-mm section for all cast numbers.

Silicon content and preheating temperature do not show a clear impact on nodule count as indicated in Figure 5a, b. Error bars show the experimental standard deviation. The standard deviation for nodule count determined from five metallographic pictures ranges from 8 to 50 nodules/mm². The highest nodule counts in the 20-mm section are found for preheating temperatures 350 and 450 °C, while in the 30-mm section, the highest nodule counts are found for 300 and 350 °C. Silicon does not show a distinct influence on nodule count because of the constant carbon equivalent and the absence of carbides in all casting sections analyzed. The impact of preheating temperature is negligible because of the large temperature difference between melt and mold. The nodule count is also influenced by other parameters like the casting temperature, which varies between 1363 and 1410 °C within all casting trials.

The pearlite content analyzed ranges from 3 to 38% in the present study. Pearlite content is always lower in the 30-mm-thick section than in the 20-mm-thick section for the same cast number. A higher silicon content leads to a lower pearlite content in the microstructure. Figure 5c, d shows the influence of Si content and preheating temperature on the pearlite content in the 20- and 30-mm-thick section, respectively. Both an increasing Si content and preheating temperature decrease the pearlite content. For 4.3 wt% Si, the pearlite percentage is lower than 10% for all preheating temperatures in the 30-mm-thick section and for all temperatures except 300 °C in the 20-mm-thick section. For 3.2 wt% Si, the pearlite percentage is always higher than or equal to 10%. For the intermediate Si

Table 4. Results of Cooling Curve Analysis

Cast no.	Wall thickness 20 mm			Wall thickness 30 mm		
	Solidification time (s)	Cooling rate (°C/s)	T_{trans} (°C)	Solidification time (s)	Cooling rate (°C/s)	T_{trans} (°C)
1	57.0	3.073	734.7	108.8	2.754	758.0
2	41.7	4.109	751.9	76.9	3.881	788.1
3	54.1	3.425	772.8	90.7	3.208	814.3
4	48.2	3.121	741.3	84.9	3.117	765.8
5	51.2	3.510	771.1	96.2	3.285	794.1
6	44.1	4.433	800.2	79.4	3.579	820.2
7	62.6	2.463	741.7	118.3	2.234	765.8
8	42.5	3.516	784.7	78.2	2.960	798.7
9	55.0	3.406	807.0	97.8	3.107	824.5
10	72.3	2.164	759.7	117.5	2.159	772.8
11	45.5	3.120	788.0	82.7	2.715	799.4
12	46.7	3.464	812.4	91.1	3.057	825.9

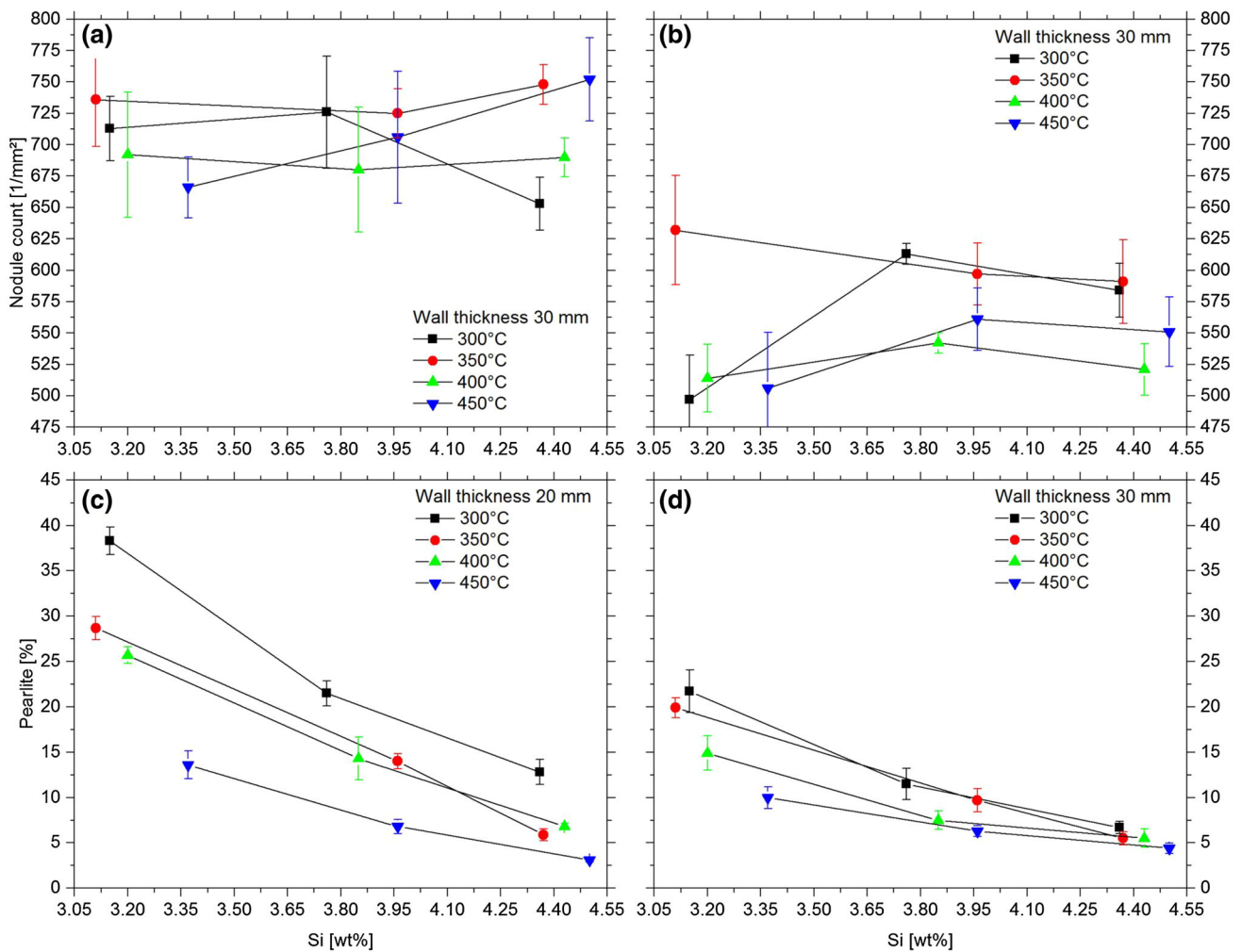


Figure 5. Nodule count for (a) 20-mm and (b) 30-mm-thick section and pearlite area fraction for (c) 20- and (d) 30-mm-thick section. Error bars indicate the experimental standard deviation.

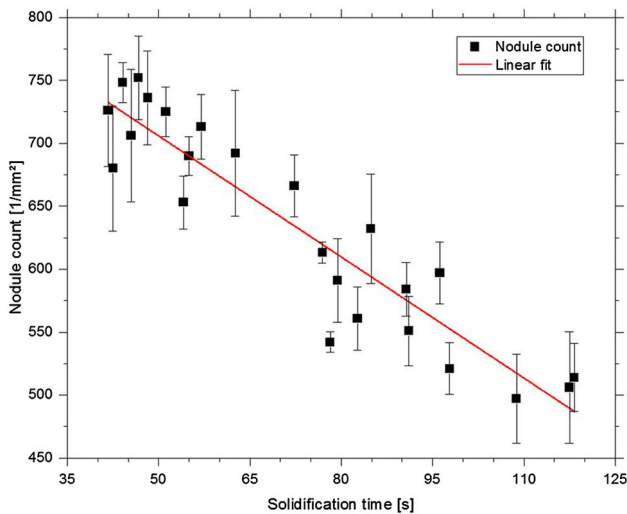


Figure 6. Correlation between solidification time and nodule count in all samples analyzed.

content of 3.8 wt%, the pearlite percentage is lower than 10% in the 30-mm-thick section for preheating temperatures of 350 °C or higher. In the 20-mm-thick section, such a low pearlite content is only reached for the highest preheating temperature. The results are in agreement with the data from Kitsudo et al.,⁸ where pearlite contents below 10% were only found for Si contents of 3.7 wt% or higher when manganese was added between 0.15 and 0.25 wt%.

The microstructures analyzed were all predominantly ferritic with a nodule count between 500 and 750 nodules per mm². The nodule count is thus considerably higher compared to the results presented by other authors.^{9,11} Narendranath and Srinivasan found 100–400 nodules per mm² for mold wall thicknesses between 19 and 32 mm. The reason for the larger number of nodules in the present study is probably a higher heat extraction rate and a more

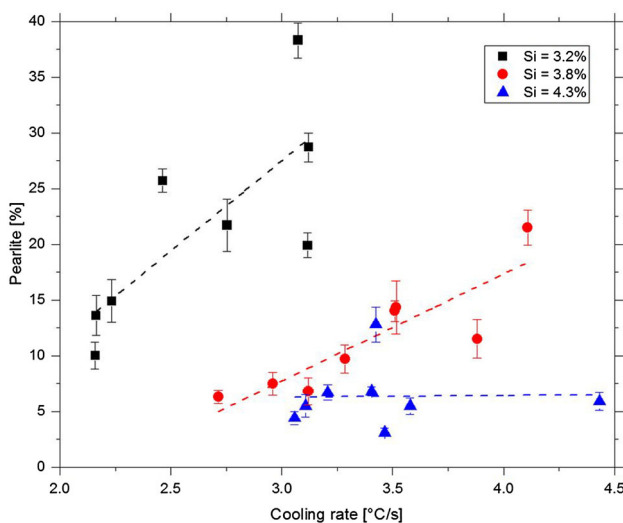


Figure 7. Impact of cooling rate on the amount of pearlite for different silicon contents.

effective inoculation process. Nevertheless, a clear correlation between nodule count and solidification time exists, which is indicated in Figure 6. The linear fit shows a good accordance with the measured data. The linear regression formula for the nodule count N_N is

$$N_N [\text{mm}^{-2}] = 866 - 3.21 * t_{\text{sol}} [\text{min}] \quad R^2 = 85.9\%$$

The reason for the found linear relationship between solidification time and N_N is probably the small interval of solidification times analyzed. Borrajo et al. analyzed the nodule count for solidification times between 0 and 700 s in thin-wall ductile iron castings and found that a power law is suitable to describe the relationship between the two parameters.¹⁵

The pearlite content is essentially affected by two parameters in the present study: the silicon content and the cooling rate in the austenitic regime. An increasing Si content increases the temperature interval in which ferrite can grow without the formation of pearlite according to Lacaze et al.¹⁶ Thus, an increase in Si decreases pearlite content in the as-cast microstructure. A higher cooling rate on the contrary promotes the formation of pearlite. When the cooling rate is high, there is less time for the depletion of dissolved carbon in austenite. An increase in cooling rate leads to an increase in undercooling of the ferritic reaction and thus to the formation of pearlite as it is analyzed by Sertucha et al.¹⁷ In the present study, it is found that the impact of cooling rate on the amount of pearlite decreases with increasing Si content. Figure 7 shows the impact of cooling rate on the amount of pearlite for the three different Si contents analyzed. The slope of the trend lines decreases with increasing Si content, and for 4.3 wt% Si no significant impact of cooling rate on the amount of pearlite is visible. The cooling rates analyzed are

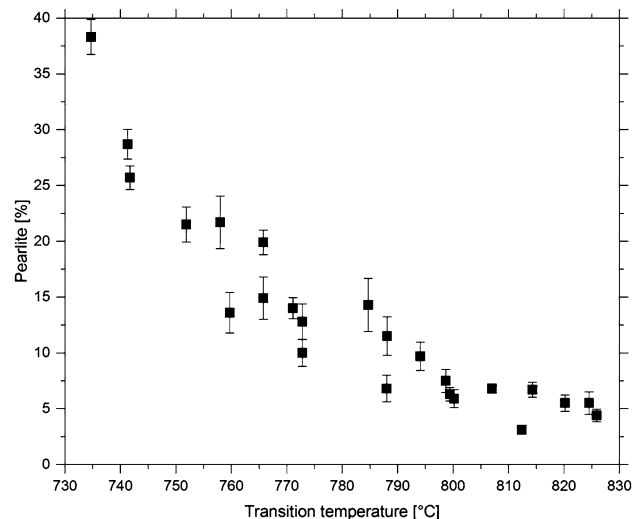


Figure 8. Correlation between experimental transition temperature and pearlite content in all samples analyzed.

apparently too low to produce significant amounts of pearlite for 4.3 wt% Si. The temperature interval for the transformation of austenite to ferrite is increased by silicon; thus, the material can tolerate higher cooling rates and higher undercooling without pearlite formation. Furthermore, Figure 7 indicates that the measured cooling rates shift to higher values when silicon is increased. This is because the cooling rate is determined in the temperature interval between end of solidification and eutectoid transformation temperature. The latter shifts to higher temperatures when silicon is increased, which tends to result in a higher cooling rate. The high scattering of data plotted in Figure 7 is due to other parameters affecting pearlite fraction such as the nodule count.

The transition temperature at which austenite decomposes into ferrite decreases when cooling rate increases or when silicon content is lowered as it is denoted by the data in Table 4. The eutectoid equilibrium temperature decreases when the Si content is lowered, whereas an increase in cooling rate increases eutectoid undercooling. When the transition from austenite to ferrite occurs at lower temperatures, carbon diffusion in ferrite is decelerated, which leads to an enrichment of carbon in austenite and thus to the decomposition of austenite into pearlite. The measured solid-state transformation temperature shows a good correlation with the pearlite content, as indicated in Figure 8. A similar connection between T_{trans} and matrix composition is presented by Sertucha et al. for copper-alloyed DI.¹⁷ Although the Si content in the present study varies between 3.2 and 4.3 wt%, the pearlite content in the as-cast microstructure seems to depend only on the transition temperature and not on the chemical composition. This is because the recorded transition temperature depends on silicon content and cooling rate. To separate the impact of silicon and transition temperature on the amount of pearlite, eutectoid undercooling is calculated. For the three

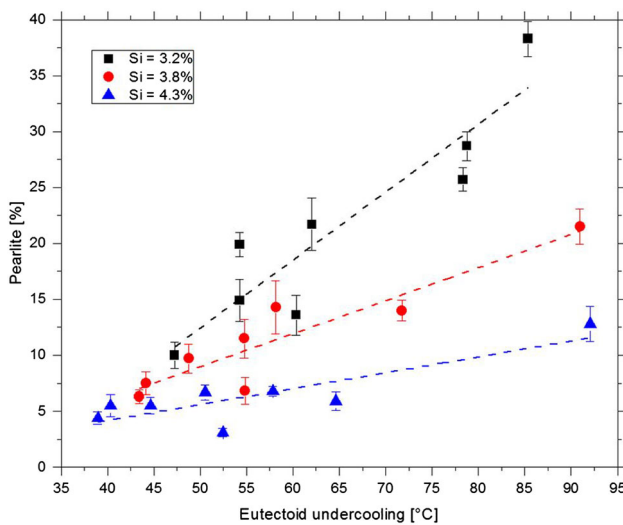


Figure 9. Impact of eutectoid undercooling on pearlite fraction for different Si contents.

different Si contents analyzed, the eutectoid equilibrium temperature T_{α} is calculated using ThermoCalc software and the thermodynamic database TCFE8. T_{α} is given by the intersection of the extrapolation of the austenite/ferrite boundary with the lowest limit of the three-phase field austenite/ferrite/graphite.¹⁶ Eutectoid undercooling is calculated by subtracting the measured transition temperature from the calculated equilibrium temperature. T_{α} is 820, 843 and 865 °C for 3.2, 3.8 and 4.3 wt% silicon, respectively. Figure 9 shows the impact of calculated eutectoid undercooling and silicon content on pearlite fraction. Compared to Figure 7, the mean variation of data is considerably reduced.

Calculated eutectoid undercooling ranges from approximately 40 to 90 °C. The results for eutectoid undercooling presented are comparable to the results of Sertucha et al.¹⁷ at similar cooling rates. Figure 9 clearly indicates that an increase in eutectoid undercooling increases pearlite fraction. The slope of the linear regression line decreases when Si increases. This mutual influence of undercooling and silicon on pearlite fraction is quantified via multiple linear regression, which leads to the following formula:

$$\%P = (1 - 0.186 * Si) * (T_{\alpha} - T_{trans}) - 4.66$$

$$R^2 = 92.1\%$$

Conclusions

The aim of this work was to find suitable conditions for the production of high-silicon ductile iron with a ferritic matrix in the as-cast state via permanent mold casting. SSDI with silicon content between 3.2 and 4.3 wt% was cast in a gray iron permanent mold with different wall thicknesses for various preheating temperatures. The cooling curves recorded via thermocouples in the mold were used to develop quantitative relationships between cooling conditions and microstructure. The results lead to the following conclusions:

1. High-silicon ductile iron can be used to produce carbide-free castings in permanent mold with a wall thickness of 20 or 30 mm. For a wall thickness of 10 mm or less, a carbide-free microstructure cannot be produced under the conditions analyzed in this paper.
2. Pearlite content in the as-cast microstructure can be reduced by increasing mold preheating temperature and silicon content. A pearlite content below 10% can be achieved for different combinations of Si and preheating temperature in wall thicknesses of 20 and 30 mm if the material contains at least 3.8 wt% silicon. A fully ferritic matrix (< 5% pearlite) can only be achieved with 4.3 wt% silicon and 450 °C preheating temperature.

3. Solidification time and nodule count are strongly correlated with permanent mold ductile iron castings. A linear dependency between solidification time and nodule count is found in the present study. An impact of preheating temperature and silicon content on the nodule count is not found because of the large temperature difference between mold and melt and the constant carbon equivalent.
4. Pearlite fraction increases when the solid-state transformation takes place at lower temperatures. The pearlite fraction can be described as a function of silicon content and eutectoid undercooling.

The results show that the SSDI materials are particularly suitable for permanent mold casting. The fact that a minimum Si content of 3.8 wt% is necessary to produce a ferritic matrix with less than 10% pearlite in the present study is probably due to the relatively high Mn content of 0.17 wt% in the base melt. The section sizes in the mold used in the presented study are not suitable to determine critical cooling conditions for carbide formation since the 20-mm step showed a completely stable solidification in all casting trials, while the 10-mm step always contained eutectic carbides. For future investigations, the thickness of the smallest step could be increased to, e.g., 15 mm to analyze this metallurgical problem.

Acknowledgements

The authors like to thank the Industrielle Gemeinschaftsforschung IGF for the funding of this research project (Project No. 18555 N). The authors gratefully acknowledge the Georg Fischer GmbH in Mettmann for supplying us with raw material for the SSF DI production, the ASK Chemicals GmbH for supplying us with facing coat, master alloys and inoculants, and the H. Brüggemann GmbH for manufacturing the permanent mold used in the present study.

REFERENCES

1. M.S. Ramaprasad, M.N. Srinivasan, in *Science and Technology of Casting Processes*, ed. By M.N. Srinivasan (Lamar University, USA, 2012). <https://www.intechopen.com/books/science-and-technology-of-casting-processes>
2. W. Stets, H. Löblich, G. Gassner, P. Schumacher, *Int. J. Metalcast.* **8**, 35–40 (2014)
3. P. Weiß, A. Tekavcic, A. Bührig-Polaczek, *Mater. Sci. Eng. A* **713**, 67–74 (2018)
4. P. Weiß, J. Brachmann, A. Bührig-Polaczek, S.F. Fischer, *Mater. Sci. Technol.* **31**, 1479–1485 (2015)
5. M. Riebisch, P. Weiß, C. Cremer, I. Aboulkhair, A. Bührig-Polaczek, *Mater. Sci. Technol.* **1**, 1–6 (2017)
6. M. Riebisch, H. Groß, B. Pustal, A. Bührig-Polaczek, *Int. J. Metalcast.* **12**, 106–112 (2018)
7. K. Jalava, K. Soivio, J. Laine, J. Orkas, *Int. J. Metalcast.* **1**, 1–7 (2017)
8. T. Kitsudo, Y. Kawano, K. Fujita, S. Kurose, *Jpn. Foundrym. Soc.* **53**, 453–459 (1981)
9. J. Khalil-Allafi, B. Amin-Ahmadi, *J. Iron Steel Res.* **18**, 34–39 (2011)
10. X. Pengju, L. Wenhua, *Foundry Tech.* (2002). http://en.cnki.com.cn/Article_en/CJFDTOTAL-ZZJS200204005.htm
11. C.S. Narendranath, M.N. Srinivasan, *J. Test. Eval.* **23**, 281–287 (1995)
12. G. Zhuyao, W. Sizeng, *Foundry Technology*, p. 01 (1990)
13. K. Herfurth, R. Gorski, K. Beute, M. Hering, *Giesserei* **98**, 68–79 (2011)
14. R.E. Ruxanda, D.M. Stefanescu, T.S. Piwonka, *AFS Trans.* **110**, 1131–1147 (2002)
15. J.M. Borrajo, R.A. Martinez, R.E. Boeri, J.A. Sikora, *ISIJ Int.* **42**, 257–263 (2002)
16. J. Lacaze, J. Sertucha, L. Magnusson Aberg, *ISIJ Int.* **56**, 1606–1615 (2016)
17. J. Sertucha, P. Larrañaga, J. Lacaze, M. Insausti, *Int. J. Metalcast.* **4**, 51–58 (2010)